Nuclear Instruments and Methods in Physics Research A 1082 (2026) 170908

Contents lists available at ScienceDirect

Nuclear Inst. and Methods in Physics Research, A

journal homepage: www.elsevier.com/locate/nima

Full Length Article

# Digital electronics upgrade of the INDRA 4$\pi$ charged particle detection array and resulting performance improvements

J.D. Frankland [a,*], N. Le Neindre [b], M. Henri [a,1], C. Gouyet [a], R. Revenko [a], Q. Fable [b,2], D. Gruyer [b], R. Bougault [b], A. Chbihi [a], T. Genard [a], J. Lemarié [a,3], O. Lopez [b], Q. Beaudouin [a], B. Borderie [c], P. Bourgault [a], C. Ciampi [a], I. Dekhissi [b], V. Godefroid [a], M. La Commara [g,h], L. Leterrier [b], E. Loubeau [a], F. Marie-Saillenfest [a], C. Nicolle [a], F. Noury [b], M. Parlog [b,f], J. Perronnel [b], M. Prieur [a], A. Rebillard-Soulié [b], L. Rousseau [a], A. Valente [b], G. Verde [d,e]

[a] *Grand Accélérateur National d'Ions Lourds (GANIL), CEA/DRF-CNRS/IN2P3, Boulevard Henri Becquerel, F-14076 CAEN, France*
[b] *Normandie Université, CNRS/IN2P3, ENSICAEN, Laboratoire de Physique Corpusculaire, F-14076 CAEN, France*
[c] *Université Paris-Saclay, CNRS/IN2P3, IJCLab, 91405 ORSAY, France*
[d] *INFN - Sezione di Catania, 95123, CATANIA, Italy*
[e] *Laboratoire des 2 Infinis - Toulouse (L2IT-IN2P3), Université de Toulouse, CNRS, UPS, F-31062 TOULOUSE Cedex 9, France*
[f] *"Horia Hulubei", National Institute for R&D in Physics and Nuclear Engineering (IFIN-HH), P. O. Box MG-6, Bucharest Magurele, Romania*
[g] *Dipartimento di Farmacia, Universitá di Napoli 'Federico II', 80131 NAPOLI, Italy*
[h] *INFN-Sezione di Napoli, 80126 NAPOLI, Italy*

ARTICLE INFO

*Keywords:*
Heavy-ion collisions
Charged particle detection and identification
Digital electronics
Acquisition system

ABSTRACT

INDRA is a 4$\pi$ charged particle detection array in use since 1993 for the study of nuclear collisions at bombarding energies from a few 10s to a few 100s of MeV/nucleon. Originally equipped with custom electronics using the VXI standard, the entire acquisition system was recently upgraded to a fully digital system using commercially-available modules supplied by mesytec GmbH & Co. KG. At the same time, both low and high voltage supplies and all cabling and signal routing outside of the reaction chamber have also been replaced. The new electronics were used for the first time in 2022 in an experiment at GANIL coupling INDRA with 12 blocks of FAZIA telescopes placed at forward angles. The full details of the upgraded system, and the resulting improvements in performance, stability, dead time and identification capabilities are presented in this article.

## 1. Introduction

Heavy-ion collisions provide a powerful tool for compressing and heating nuclear matter, offering unique insights into its behaviour under extreme conditions. The reaction dynamics are primarily influenced by the mass, charge, and energy of both the projectile and target. Comprehensive studies in this field require a wide range of projectile–target combinations and incident energies, spanning from a few MeV to 100 MeV per nucleon. The large number and variety of nuclear species emitted at these energies, especially in central collisions, require arrays with not only 4$\pi$ solid angle coverage but also high granularity and large dynamic range in both identification and energy measurement capability.

The INDRA detector [1] was specifically designed to investigate the dynamics of N-body open quantum systems [2], the equation of state (EOS) of nuclear matter [3], clusterization and multifragmentation phenomena, and the thermodynamic properties of finite systems [4]. INDRA (the initials are from the French "Identification de Noyaux et Détection avec Résolutions Accrues", or "Identification of Nuclei and Detection with Enhanced Resolutions" — INDER — in English) was built at the beginning of the 1990s as one of the second generation 4$\pi$ detection arrays for charged particles, with characteristics optimized for the study of heavy-ion collisions using the beams and energies available at GANIL, able to detect and characterize all charged products from protons of ~1 MeV up to Uranium ions of ~4 GeV. This places strong constraints on the electronics to be used with such an array, in

* Corresponding author.
*E-mail address:* john.frankland@ganil.fr (J.D. Frankland).
[1] Current address: CEA/INSTN/UECC, 143 Chemin de la Crespinière – ZA Les Vindits, F-50130 CHERBOURG EN COTENTIN, France.
[2] Current address: GANIL, CEA/DRF-CNRS/IN2P3, Boulevard Henri Becquerel, F-14076 CAEN, France.
[3] Current address: RIKEN, Nishina Center, Wako-shi, 351-0198, Saitama, Japan.

https://doi.org/10.1016/j.nima.2025.170908
Received 20 February 2025; Received in revised form 4 July 2025; Accepted 26 July 2025
Available online 9 August 2025

terms of the elevated number of channels to be handled, the means of triggering the associated data acquisition system (DAQ) to record the data coming from many different channels for each collision, and maintaining large dynamics without sacrificing resolution.

In order to record the signals produced by the 96 ionization chambers (ChIo), 192 silicon (Si) detectors, 324 CsI(Tl) scintillators read out by photo-multiplier tubes and 12 NE102(500 μm)/NE115(25 cm) phoswich detectors[4] of the original array, custom-made electronics modules based on the VXI (VME Xtensions for Instrumentation) standard were developed specifically for INDRA [5]:

- for the Si and ChIo detectors:
  - 7 48-channel constant fraction discriminator (CFD) modules;
  - 10 32-channel dual-range charge integrating ADC modules, with 12-bit resolution for both outputs;
- for the CsI(Tl) detectors:
  - 14 24-channel modules combining CFD and dual-gate ADC integration, with 12-bit resolution for the fast and slow gate outputs;
- for the 12 phoswich telescopes (see footnote 4):
  - 1 12-channel module based on a modified version of the CsI electronics providing a similar dual-gate integration [6];
- for all detectors:
  - 7 96-channel modules to provide individual time markers for each fired detector with a precision of 10 ns (10-bit resolution), relative to the trigger of each event.

In addition, 2 dedicated modules were developed to handle event triggering, data readout and liaison with the data acquisition system.

These 41 modules were housed in 4 size D VXI crates, alongside 3 CAMAC crates containing 59 custom 8-channel modules (38 variable gain amplifiers and 21 variable amplitude pulser modules for the Si and ChIo detectors) and 3 NIM crates containing the 30 custom modules of the "regrouper" system which generated multiplicity signals and non-programmable logic functions of the trigger (ensuring recording of coincidences in the ChIo-Si/CsI telescopes). Last but not least, the high voltage supplies for all detectors were provided by 8 CAEN crates each handling 64 individual channels, while low-voltage supplies for Si and ChIo preamplifiers were provided by separate custom-made modules. The full setup was housed in 5 full-sized bays with a dedicated air conditioning plant that was essential during operation in order to evacuate the heat generated by the different crates, especially VXI and CAMAC.

At the time, for an array of 628 detection channels, the INDRA electronic system was seen as a cutting-edge system in nuclear physics, not only in terms of its (relative) compactness, but also for the fact that the vast majority of the settings for the different channels could be performed remotely by computer, thus allowing the whole electronics to be installed inside the experimental cave dedicated to INDRA at GANIL, D5. Not only was it used successfully for more than 25 years for every experiment performed with INDRA (up to and including the first experiment with the coupled INDRA-FAZIA setup in 2019 [7]), but, remarkably, the whole installation was relocated twice during its history, the first time in 1998/9 for the fourth INDRA campaign at GSI [8], and then again in 2007 for two experiments coupling INDRA with the VAMOS spectrometer [9,10] in an experimental cave (G1) on the other side of the GANIL experimental areas. INDRA has also been used to measure the fission time as a probe into superheavy element stability [11].

By 2019 and the first INDRA-FAZIA experiment, the electronics were suffering an increasing number of failures. The removal of the first five rings of INDRA in order to install the FAZIA demonstrator liberated a temporary supply of spare VXI modules. The high voltage supplies had been similarly afflicted for many years, and only by further reducing the number of channels could they continue to be fit for purpose; low-voltage supply modules were also beginning to fail.

In 2020 the number of failures either of individual channels or of whole modules had become too large to ignore, and it was decided to replace the electronics outside of the reaction chamber.[5] After testing several possible alternatives for the DAQ electronics, a commercially available, off the shelf, solution proposed by mesytec GmbH & Co. KG was chosen as most suited to the needs of re-implementing a working DAQ system for INDRA. With funding obtained from the Région Normandie regional council as part of a larger envelope provided by the latter to GANIL, it was possible to carry out a complete renovation of the electronics, including low and high voltage supplies, the cables feeding out from the vacuum chamber and the signal routing boxes. A first beam test with a few mesytec modules was performed in spring 2021, following which the whole of the existing electronics were dismounted. The manufacturing of the new cables, carried out on site by both physicists and technical staff, and the installation of the new system progressed throughout 2021. The full system was tested for the first time with $\alpha$ source and cosmic rays in January 2022, and the first experiment using the new electronics, including the coupling of INDRA and FAZIA, was performed successfully in spring 2022 [12]. In this paper, we will give the technical details of the new electronics of INDRA, along with some results highlighting the improved performances of the new DAQ.

## 2. Technical details of the upgrade

### 2.1. Data acquisition electronics

In the new DAQ system, detector signal digitization and event building are handled by commercially available modules developed by mesytec GmbH & Co. KG. The entire electronics setup is contained in a single VME crate (see Fig. 1).

#### 2.1.1. Signal processing modules

At the heart of the new INDRA DAQ is the MDPP-32 module [13], a fast, high resolution time and amplitude digitizer. The MDPP-32 is internally realized as a 32 channel adjustable low noise amplifier and variable differentiation stage, followed by anti-aliasing filters and 80 MHz sampling ADCs. The digitized data are then analysed in an FPGA whose firmware can be selected at power up according to signal processing requirements. The amplitude resolution of these modules is as good as the best analogue solutions, including ballistic loss correction, pile up rejection and baseline restoration. The main features of this module are:

- low noise variable gain input amplifiers;
- 16 bit coding resolution;
- gain-polarity jumpers to easily adapt the polarity and range of the input signals;
- up to 3 different signal processing firmwares can be stored on board and selected according to requirements;

[4] Replaced from 1998 onwards by 12 Si-CsI(Tl) telescopes .

[5] It should be noted that no modifications have been made to the electronics inside the chamber, including the photo-multipliers of the CsI(Tl) scintillators and the front-end electronics (preamplifiers) of the Si/ChIo detectors which are still mounted as close as possible to the detectors, under vacuum.

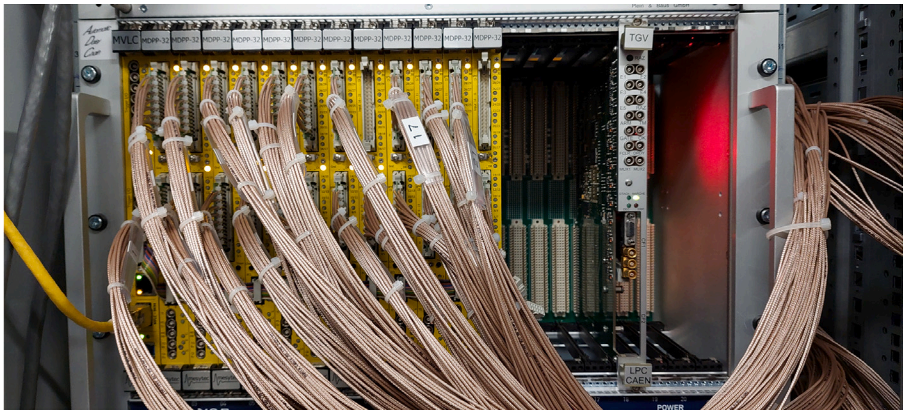


**Fig. 1.** The complete INDRA electronics for the E818 [12] experiment housed in a single VME crate: from left to right, MVLC trigger/controller, 8 MDPP-QDC modules for CsI(Tl) detectors, 4 MDPP-SCP modules for Si detectors, and the TGV module (without connections).

- individually adjustable threshold for each channel;
- 'window of interest' concept for validation of triggered channels (see below).

For INDRA, MDPP modules with two of three different firmwares are used, depending on the nature of the connected detectors:

- **SCP** firmware for standard charge sensitive preamplifier signals, such as those coming from silicon detectors and ionization chambers. The signal amplitude (energy) is encoded as a 16 bit value;
- **QDC** firmware for integration of CsI photo-multiplier signals over short and long time intervals, for pulse shape discrimination. Both integrated values are encoded with 16 bit resolution.

Both firmwares feature a timing branch which provides an amplitude-independent time trigger for each channel. They may be used either internally to trigger the module or externally to construct a global event trigger. See [13] for full details of the firmwares.

The window of interest (WoI) concept is perhaps the most attractive feature of the MDPP concerning a large-scale detector array such as INDRA, as it allows to function analogously to the asynchronous trigger that was one of the major innovations of the original VXI electronics. The WoI is generated for each module by a user-definable trigger input, either internal or external, with an adjustable width (1.5 ns to 25 μs) and offset (±25 μs) with respect to the input trigger. The 32 channels of each module trigger independently, but only those whose CFD fires in coincidence with the WoI are retained when data is read out from the module. Data from validated channels then include, in addition to their signal data, the time difference between the WoI start and the individual channel trigger. The resolution of this time difference (nominally as low as 70 ps for fast signals; in the worst case, i.e. CsI photo-multiplier output, 10∼50 ns [14]) is sufficient to discriminate pile-up from different beam packets, as the GANIL cyclotrons typically operate at ∼10 MHz.

To handle the "full" INDRA setup requires:

- 11 MDPP modules with QDC firmware and jumpers adapted to 4 V full range negative polarity input signals (CsI detectors);
- 6 MDPP modules with SCP firmware and jumpers adapted to 4 V full range negative polarity input signals (Silicon detectors);
- 3 MDPP modules with SCP firmware and jumpers adapted to 4 V full range positive polarity input signals (ChIo detectors).

The required number of modules, plus spares, were purchased in 2021. The current setup, without ionization chambers and with the first 5 rings removed in order to couple with the FAZIA demonstrator, requires 8 modules for CsI detectors and 4 modules for Silicon detectors. In both cases it is possible to house the full DAQ electronics (including the MVLC VME controller/trigger module, see next section) in a standard 21-slot VME crate (Fig. 1).

#### *2.1.2. DAQ trigger*

The DAQ electronics in the VME crate is controlled by an MVLC module [15]. This is a modern, FPGA-based VME controller enabling readout at high trigger and data rates. It is easily configured and operated using an open-source software package provided by mesytec, which includes a graphical user interface for setting up and running an acquisition [16]. As well as communicating with the MDPP modules in the crate via the VME bus, the MVLC provides 14 lemo connectors on its front panel which are software-configurable as either trigger inputs (NIM or TTL) or trigger outputs/gate generators (NIM), and an additional 3 LVDS outputs which can be connected to corresponding connectors on the MDPP modules.

The basic logic of the trigger system for the DAQ is shown in Fig. 2. For each MDPP module in the setup, it is possible to generate a logical OR of any combination of the triggers of the individual channels and transmit it over one or more of the IRQ lines of the VME backplane (up to a maximum of 6 IRQ lines may be used). The IRQ signals can then be used as inputs for the programmable logic of the MVLC trigger. In our setup, the OR of all ChIo triggers are transmitted on one IRQ line, the OR of all Silicon triggers on another, while for the CsI triggers two IRQ lines are used, one for rings 1 to 12 ($\theta < 90^o$) and another for rings 13–17 ($\theta > 90^o$).

The global event trigger is then constructed as the logical OR between one or more of the IRQ lines for different detector types (for example, in the current setup, we use the OR of all Silicon detectors and all CsI detectors which can be constructed from the 3 corresponding IRQ inputs of the MVLC). Triggers are then validated if the DAQ is not already occupied by a previous event, i.e. in dead time. In our case, the dead time has two contributions: first, after a validated trigger, it is necessary to wait around 7-8 μs for the MDPP modules to finish signal processing and be ready for readout (this delay is included in the programmed trigger logic; we delay the beginning of the module readout for 8 μs); after this, a minimum of 6-7 μs is required for the readout of the modules in our setup. Thus, when the system is not in dead time, the event trigger is validated and transmitted over the LVDS output to each module in order to trigger its WoI and validate any channels which fired within a time window corresponding to the same reaction which generated the event trigger. Typical WoI widths used are 250 ns for the CsI modules, 500 ns for Silicon and 3 μs for ChIo.

#### *2.1.3. Integration with GANIL run control*

To use the new INDRA DAQ at GANIL requires an interface with the NARVAL [17] run control system used to handle dataflows from different acquisition systems up to the production of final raw data files on disk in a standardized format known as MFM [18]. This has been achieved in three stages, requiring several (but less than four) years of development:

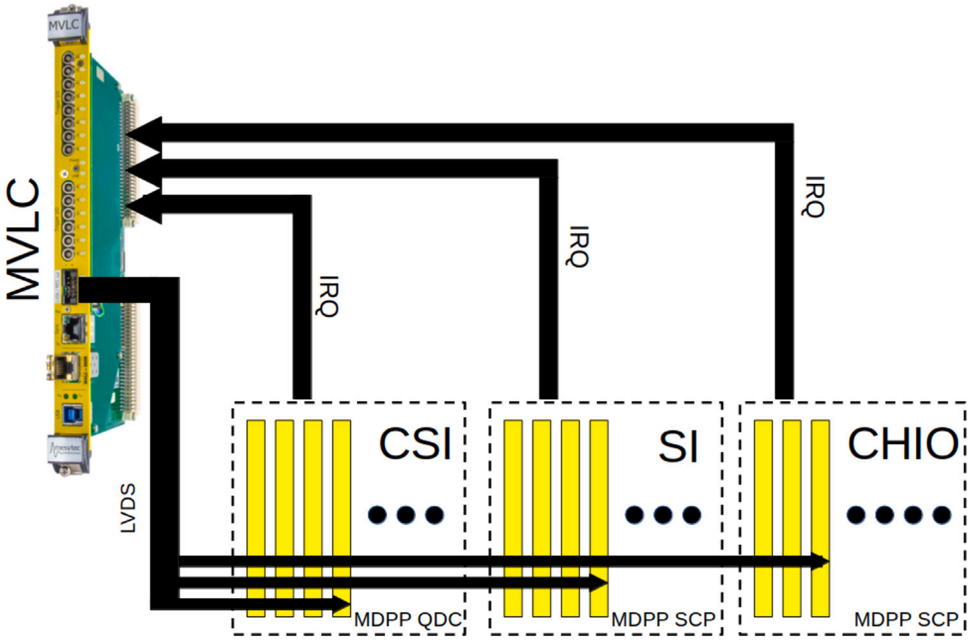


**Fig. 2.** Schematic of the basic DAQ trigger logic: the logical OR of the individual channels' CFD for modules handling different types of detector are transmitted over the IRQ lines of the VME backplane to the MVLC in order to generate the event trigger; if validated, the MVLC transmits a validated trigger over the LVDS connectors to generate a synchronous WoI for each module. See text for explanations of acronyms.

- development and integration into the Mesytec DAQ software of an option to transmit events over a ZeroMQ socket [19];
- development of a transceiver (C++ library and application) [20] capable of receiving the DAQ events on a ZeroMQ socket, encapsulating them into an (Mesytec-specific) MFM container, and retransmitting the resulting bufferized data on another ZeroMQ socket;
- development of a NARVAL actor in C++ [21] which can receive MFM data from a ZeroMQ socket and inject it into the dataflow.

*2.1.4. Coupling with other DAQ systems*

To make it possible to couple the new DAQ with that of other detectors such as FAZIA [22] requires the ability to attribute a common event number or timestamp to the events coming from each subsystem. In the present case of INDRA and FAZIA, the coupling is achieved by distributing timestamps to both subsystems from a common universal clock provided by a CENTRUM module [23] housed in a separate dedicated VXI crate. The timestamp has a 10 ns resolution and contains 48 bits (providing continuously increasing clock values for just over a month if necessary). In the case of INDRA, the distribution is assured by the addition of a specific VME module (TGV, for "Trigger Générique VME"), developed at LPC Caen and GANIL, in the crate containing the MVLC. Each validated event trigger is fed out from one of the 14 lemo connectors of the MVLC to the trigger input of the TGV module; this causes the TGV to request a timestamp from the CENTRUM (via a connecting cable). The received timestamp is then read from the TGV module using an appropriate VME script added to the MVLC trigger programme, and included in the data produced by each event as a "pseudo-module" with an identifier which is specific to the TGV. The transceiver [20] recognizes the TGV identifier and sets the timestamp in the MFM frame header according to the data received. The events from the different subsystems corresponding to the same reaction can then be merged together within the NARVAL dataflow using a suitable Merger actor [24].

*2.1.5. Scalers*

The MVLC trigger/controller module also provides 8 user-configurable 64 bit counter registers which can be used instead of a separate scaler module. We have implemented the use of these scalers in a similar way to the TGV module, i.e. data read out from each scaler is injected into the DAQ data stream with a 'pseudo-module' address so that they may be decoded and transmitted in the transceiver [20]. In order to decouple the scaler readout from the event rate fluctuations, the scalers may be read out according to an independent timer, say every second. The data flow coming from the transceiver and received by the NARVAL run control then contains MFM frames of two types, either containing data from the electronics (with a timestamp), or containing only the values of the scalers (no timestamp).

*2.2. Power supply electronics*

Low and high voltages are required both to power the in-vacuum electronics (preamplifiers and photo-multiplier tubes), and polarize the detectors (ionization chambers and silicon detectors) of INDRA. The wide range of biases, from ±12 V to $\sim -2000$ V, distributed sometimes through the same connector and the large number of channels, oriented us towards a compact and integrated modular system for sake of simplicity. The retained solution was chosen as a single CAEN crate SY4527 type [25]. It features a front side 5.7″colour LCD touch screen for local control/display and a remote control showing all channels independently on the same interface. At the rear, this crate can host up to 16 slots to plug/connect HV modules of different types described in more details below. Total dimensions are 36x48,3 cm.

- CsI(Tl) photo-multipliers:
  To supply the negative voltages (from −1000 to $\sim -2000$ V) towards the 336 photo multipliers of different size, glued on the crystals, 7 CAEN A7030N 48-channel modules [26] are necessary. Each channel is able to reach −3000 V and 1 mA. The voltage channels are set independently and current monitoring is available too.
- Si detectors:
  60 voltage channels are necessary to bias the 192 INDRA silicon detectors ranging from 2 ° to 45 ° (rings 1 to 9). They are supplied by 2 CAEN A7040AN 48-channel modules [27], able to deliver up to −100 V and 1 mA per channel.

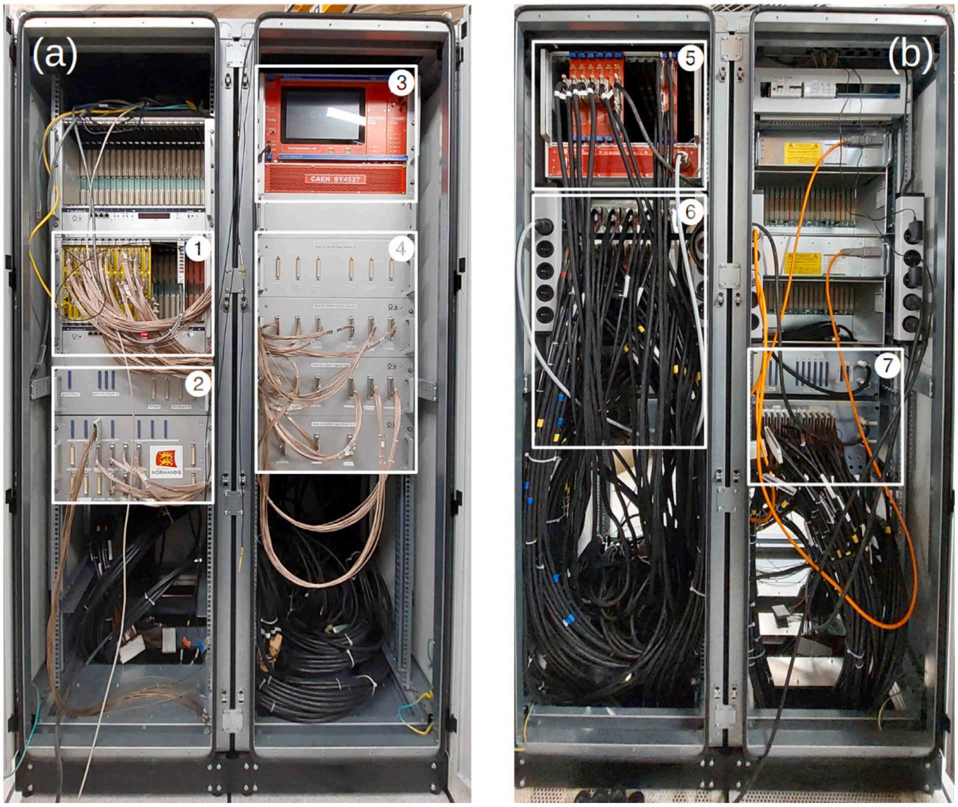


**Fig. 3.** The ATOS temperature-controlled units containing the upgraded electronics, (a) front view, (b) rear view (front and rear doors open). The numbered boxes in the picture indicate: (1) VME crate containing mesytec electronics and TGV module (see 2.1.4); (2) signal output connectors on routing boxes for silicon and ChIo detectors (see 2.3); (3) CAEN high- and low-voltage supply crate (see 2.2); (4) signal output connectors on routing boxes for CsI detectors (see 2.3); (5) rear of CAEN crate showing individual high- and low-voltage modules (see 2.2); (6),(7) rear of CsI and Si/ChIo routing boxes showing connections of cables coming from chamber feedthroughs;.

- ChIo detectors:
  For the 96 ionization chamber cells, distributed on 5 structures covering from 2 ° to 176 °, each with a common cathode side to be polarized (the cathode corresponds to the entrance window closest to the target; the anode exit window is grounded), 5 HV supplies are required. One CAEN A1542DN 12-channel module [28] was chosen, supplying up to −500 V and 1 mA for each output.
- Concerning the on-board (front-end) electronics, under vacuum, the low voltages necessary to supply the ±12 V to the preamplifiers for both ChIo and Si detectors are delivered by 6 CAEN A2519CA 8-channel modules [29] able to power up to ±15 V and 5 A for each channel.

In total 16 HV CAEN modules are necessary to supply high and low voltages to the full INDRA setup as it was in 1993.[6] The crate is housed in the bays with the electronics in the experiment room (see Fig. 3), and all settings are fully remote controlled via Gigabit ethernet network using the GECO2020 software provided by CAEN. An interlock system is used to automatically cut the photo-multiplier voltage supply in case of vacuum failure.

### 2.3. Cabling and signal routing

For sake of simplicity and since the cabling and routing inside the vacuum chamber are very compact and integrated, it was preferred not to change their layout. This also means that the connection feedthroughs on the flanges were kept as they were designed back in the 1990s. On the contrary, the external (in air) cables and connectors were all rebuilt from scratch.

Before dismounting the old external cables and electronics a huge effort was made to document the whole connection layout, detector signals, ground lines, high and low voltages, pulser lines, flanges (with a mix of 53-pin and 29-pin connectors) ... pin by pin on the various feedthroughs. The whole documentation has been rewritten taking into account the specifics of the new electronics and power supply modules. Once this work was complete, the new external layout design started. A new interface between the electronics inputs and the mixed signals/power supply exiting from the flanges on the vacuum chamber has been engineered. It consists of four router boxes for the CsI(Tl), two boxes for the Si/ChIos and an additional one for low voltages. Their goal is to dispatch and reorganize the signal inputs-outputs that are mixed on the same cable/connector (arriving at the rear of the boxes: see Fig. 3(c)) in a more user friendly way, by type of detector, power supply, pulser inputs and location (by INDRA ring) on the front side. The signal routing boxes were built by ATOS company [30] and all inside cabling/routing and connector housing was designed and installed at LPC Caen.

In total 174 cables, each made up of 8 individual coaxial cables, connect the chamber feedthroughs to the signal routing boxes, each between 8 and 11 metres long, according to the location of the feedthrough on the vacuum chamber. These were provided by Ivry Interconnect Services (2IS), now part of Agilink Group [31]. Cables were prepared individually onsite in the D5 cave, using both new and reconditioned connectors from the original electronics. Indeed taking care of correct grounding, signal and power supply transmission, the Socapex [32] connectors used previously were still the best solution, able to handle at the same time signals of a few kV (CsI(Tl) PM HV supply) and a few mV (e.g. silicon detector preamplifier signal). On the other hand, new multi layers PCBs were designed for the

[6] For the current setup, 5 modules are required for CsI/PM HV, 1 module for Si polarization, and 2 modules for Si preamplifier low voltages.

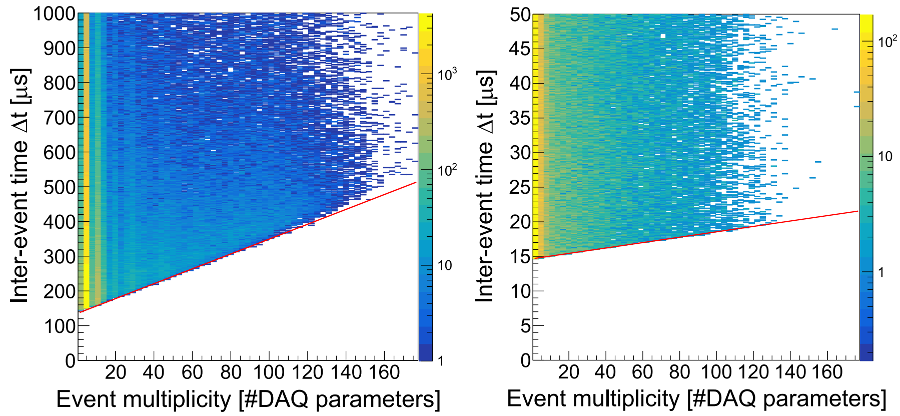


**Fig. 4.** Experimental data from two experiments: E789 [7] using the original VXI-based DAQ system, and E818 [12] using the new mesytec digital electronics. The time between two successive acquired events, $\Delta t$, is plotted as a function of the number of DAQ parameters in the first event, with a logarithmic colour scale representing the number of events (note the factor of 20 difference in the *y*-axis scale between E789 and E818). The red lines represent 1st order polynomial fits to the minimum value of $\Delta t$ for each event multiplicity. The parameters of the fits are given in Table 1.

connectors according to the new layout design insuring good quality grounding and low electronics noise. In total, close to 2 km of cable were necessary, along with nearly 250 different connectors. Finally, the cables connecting the CAEN modules to the routing boxes were supplied by CAEN, and the cables connecting the MDPP modules were supplied by mesytec.

The whole ensemble (electronics modules, power supply, VME chassis, routing boxes...) is placed inside two cooling cabinets (dimensions: H = 2.1 *x* D = 1.2 *x* W = 1.0 m) regulating the temperature at around 20 °C and able to dissipate 2.0 kW at maximum. They are equipped with doors with glass windows on the front side ensuring good visibility on the electronics modules, and were supplied by ATOS company (see Fig. 3).

## 3. Measured performance improvements

### 3.1. Dead time

The first major improvement to the performance of the INDRA DAQ observed with the new digital system concerns the acquisition dead time. Let us first distinguish the two types of "dead time" which may affect any experimental measurement. The first, which we will call Intrinsic Dead Time (IDT), corresponds to the minimum time required by the electronics to treat a triggering event and subsequently be ready to treat a new event. IDT may increase with the number of fired channels, and thus the number of modules/parameters to read out after treatment, but is independent of the nature of the measurement (reaction rate, beam current, trigger rate, etc.): it is an intrinsic characteristic of the electronics. The second type, which we will call Measurement Dead Time (MDT) is a direct result of the DAQ system's IDT and can be quantified by the fraction of time during any experimental measurement in which the DAQ is unavailable to acquire new events or by the ratio between the total number of triggers and the number of validated triggers. On the contrary to IDT, MDT will depend on the nature of the measurement: in general it will increase with reaction/trigger rate and the average number of fired channels per event.

The IDT of the system can be measured if each event is assigned an absolute timestamp of sufficient resolution. Both the first experiment coupling INDRA and FAZIA in 2019, E789 [7], using the original VXI DAQ system, and the first experiment using the new mesytec digital DAQ electronics, E818 [12] used the same CENTRUM module to provide timestamps to both arrays (see 2.1.4). Therefore we can measure and compare the absolute IDT of the old and new DAQ systems using the data from the two experiments.

**Table 1**
A Measured intrinsic dead time (IDT) for the original (old) DAQ electronics and the new setup using mesytec modules: comparison of minimum incompressible time between two acquired events and time required for the readout of each additional DAQ parameter.

| | A Minimum $\Delta t$ [μs] | Readout time [ns] |
|---|---|---|
| old DAQ | $136.8 \pm 0.7$ | $2098 \pm 11$ |
| new DAQ | $14.65 \pm 0.03$ | $39 \pm 0.4$ |

The comparison is presented in Fig. 4. For each successive pair of events $\mathcal{E}_i$ and $\mathcal{E}_{i+1}$ in the data, we calculated the inter-event time $\Delta t$ from the difference in the timestamps of the two events. This time difference is plotted as a function of the total number of DAQ parameters in event $\mathcal{E}_i$. When considering the inter-event time $\Delta t$ it is important to recall that the frequency of the GANIL cyclotrons is typically of order 10 MHz, therefore the minimum time between two beam packets is of order 100 ns; inter-event times of the order of μs are therefore solely due to the limitations of the electronics. Longer inter-event times are due to the statistical nature of the reactions: in the absence of any particular time structure of the beam, the time between two events which occur with a given fixed probability (total reaction cross-section for a given combination of beam and target) should follow an exponential distribution, as for any Poisson process.

As can be seen in Fig. 4, for both DAQ systems there is a clearly defined minimum inter-event time which increases linearly with the number of DAQ parameters of the event (which is closely related to the number of fired detectors and/or the number of detected particles (multiplicity) of the event). However, there is an order of magnitude difference between the absolute minimum inter-event time observed for the smallest events with the two DAQ. This has been quantified by performing fits to the minimum $\Delta t$ for each event multiplicity with a 1st order polynomial. The results are presented in Table 1 where the IDT of both systems is quantified in terms of the minimum incompressible time between two acquired events containing a single fired detector, and the extra time required for each additional parameter.

With the original DAQ the dead time was at least ∼140 μs, increasing up to ∼500 μs, with the readout of each additional parameter adding ∼2 μs to the total dead time[7] (it should be noted that each fired detector adds 3 DAQ parameters). By comparison, the IDT of the FAZIA array is ∼10 μs. For this reason in the coupled trigger logic of E789 [7] INDRA events had to be validated by a trigger from FAZIA, i.e. only events in which FAZIA fired were accepted: reactions where only INDRA fired

[7] This measured value corresponds exactly to the value given in [5].

were rejected at the trigger level, in order to avoid the relatively huge dead time this would bring. This could be justified as the main goal of the experiment was an exclusive measurement of both $Z$ and $A$ for residues of $^{58,64}$Ni quasi-projectiles [33], which only FAZIA can achieve.

For the new DAQ system the measured IDT is only ∼15 μs, which corresponds to the readout delay programmed in the trigger logic of the MVLC plus the minimum MDPP readout time (see 2.1.2). Each additional parameter then adds only ∼40 ns to the total dead time, or ∼120 ns per fired detector, with the result that the IDT is not only far smaller in absolute value but also far less multiplicity dependent than before (the variation is only from ∼15 to ∼20 μs). As a result, for the second experiment coupling INDRA and FAZIA, E818 [12], the two DAQ now having very similar IDT, it was no longer required to veto any combination of the event triggers, and indeed it is now possible to operate INDRA-FAZIA in common dead time.

The measurement dead time (MDT) of each DAQ system was measured during both E789 and E818. In both cases, scalers were used to count, during each run:

- for E789, the total number of ticks of the internal clock of the VXI trigger module, and the number of ticks occurring while the trigger was in dead time;
- for E818, the total number of trigger requests received by the MVLC module and the total number of validated triggers.

MDT has been calculated in both cases using the ratio of these quantities for each run.

As MDT depends on the nature of the measurement, in order to compare MDT for the two experiments we have used data from runs with the most similar conditions, i.e. runs without beam, using $\alpha$ sources and with or without the CsI scintillators included in the trigger. The results are shown in Fig. 5 as a function of the acquisition rate during each run.

Runs with very different acquisition rates and MDT are observed for the E789 data: the lowest for a single-sided $\alpha$ source irradiating only the silicon detectors between 14 ° and 45 °, the highest using a double-sided source irradiating not only the silicon detectors but also the CsI scintillators from 45 ° to 176 °, with in addition detection of cosmic rays in all CsI detectors of the array. The MDT increases linearly with the acquisition rate, as indicated by the linear fit represented in Fig. 5 by a dashed line. Extrapolation of this fit suggests a MDT of 100% for acquisition rates greater that 4 kHz; unsurprisingly, such rates were never reached with the old electronics.

On the contrary during E818 only runs using the double-sided $\alpha$ source and with all silicon and CsI detectors included in the global trigger were recorded, for which an acquisition rate of ∼5 kHz could be comfortably sustained by the new electronics, while the measurement dead time remained low, ∼5 %.

### 3.2. Isotopic identification of intermediate mass fragments

We have observed a major improvement in the isotopic identification of intermediate mass fragments achieved in Si-CsI telescopes with the new set up. In previous INDRA experiments, isotopic identification was principally achieved only for the lightest nuclei ($Z < 5$) stopping in CsI crystals, using pulse shape discrimination of the CsI light output. The $\Delta E$ signal from the silicon detectors on rings 1 to 9 was almost never successfully used to provide isotopic identification of fragments[8], for several reasons. Firstly, the gain of the preamplifiers previously used was adapted for a maximum of 4 GeV energy deposition, in order to cover the full range of fragments produced with the heaviest beams at GANIL, up to $Z = 50$, and the 12 bit resolution of the analogue electronics did not then permit discrimination between different isotopes of the same element. Secondly, the total light output of the CsI detectors was not directly measured before, but numerically reconstructed from the 'fast' and 'slow' components recorded by the dedicated VXI modules (integration gates 0-400 ns and 1600-3100 ns respectively [34]). The MDPP-QDC modules used with the CsI detectors are set for 'fast' (0-400 ns) and 'total' (0-3.5 μs) gates, therefore we now have a far more direct measurement of the total light output, reducing uncertainties due to reconstruction approximations. The other major contributing factor to the improvement in the isotopic resolution comes from the automatic baseline restoration provided by the MDPP modules. This reduces noise and improves resolution by suppressing any fluctuating offset on an event-by-event basis. With the previous electronics, it was only possible to perform an average correction by performing dedicated noise measurement runs (pedestal measurement) during the experiments.

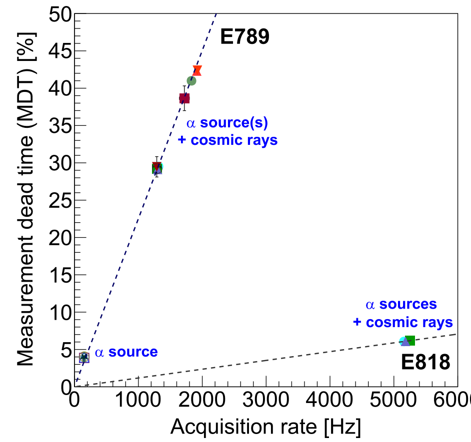


**Fig. 5.** Measurement dead time (MDT) as a function of acquisition rate measured during various runs from E789 and E818 with single- or double-sided $\alpha$ sources, and with or without CsI detectors triggering on particles from cosmic rays and/or $\alpha$ source. The dashed lines are linear fits to the dependency of the MDT on acquisition rate for each experiment.

For the first experiment with the new electronics, using beams of $^{36}$Ar or $^{58}$Ni at 74 MeV/nucleon and a further test beam of $^{84}$Kr at 68 MeV/nucleon, the sensitivity of the preamplifiers of the silicon detectors on rings 6 to 9 was increased by a factor of 4 based on the expected yields of relatively light ($Z < 20$) fragments at these angles (between 14 and 45 degrees in the laboratory). In addition, the silicon detectors of rings 6 and 7 were replaced with new 300 μm thick sensors provided by Micron Semiconductors Ltd.

Fig. 6 presents an example of $\Delta E$-$E$ correlations obtained with a typical Si-CsI telescope for the $^{84}$Kr beam impinging on a $^{124}$Sn target. Also shown in the figure is the identification grid used to linearize the data [35], with lines drawn to follow the correlation for one isotope for each $Z$ in the $\Delta E$-$E$ plane. Examples of linearized data, the distribution of the particle identification (PID) coordinate, for several elements are presented as histograms in Fig. 7.

For each element $Z$ for which isotopic identification is possible, several peaks appear in the PID spectra corresponding to different isotopes of mass $A$. We have performed multi-gaussian fits to these linearized spectra, using the following function:

$$y(x) = \sum_{i=1}^{N_g} N_i \mathcal{G}(x, f(A_i), \sigma) + \mathcal{B}(x) \quad (1)$$

where:

- $x$ is the PID coordinate;

[8] During the 5th INDRA campaign (2001), an attempt to compromise by keeping large $Z$ identification capacity while increasing preamplifier sensitivity was made by replacing a few silicon wafers on each ring with thinner 150 μm detectors, but the resulting increase in straggling effects on the energy deposit also inhibits isotopic identification.

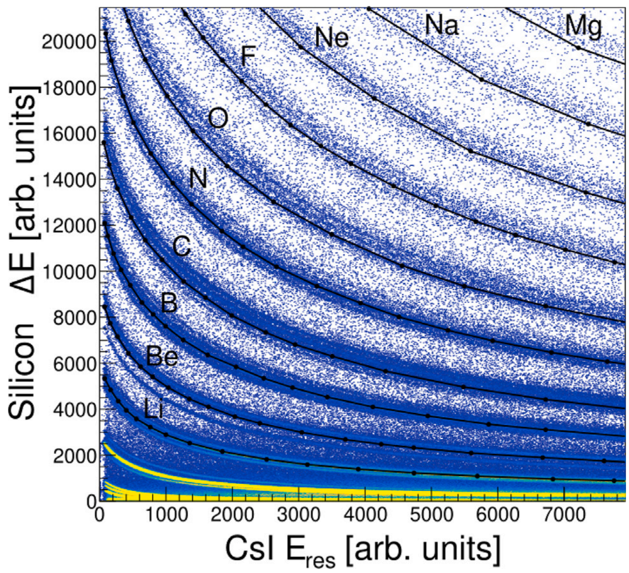


**Fig. 6.** Raw data obtained for the $^{84}$Kr(68 MeV/nuc.)+ $^{124}$Sn reaction with telescope 3 of ring 6 covering laboratory polar angles $\theta = 14{\sim}20°$ and azimuthal angles $\phi = 45{\sim}60°$. Black dots joined by lines represent the identification grid with one line per $Z$ for $Z > 2$ used to linearize the data and produce the PID spectra.

- $y(x)$ is the yield for a given PID coordinate $x$;
- $N_g$ is the number of gaussians/isotopes in the spectrum;
- $\mathcal{G}(x, \bar{x}, \sigma)$ is a normalized gaussian distribution with centroid/mean $\bar{x}$ and standard deviation $\sigma$ (the same $\sigma$ is used for all isotopes $A_i$ of a given element $Z$ for a given telescope, but $\sigma$ varies from one element to another and one telescope to another);
- $N_i$ is the yield for each isotope;
- $f(A_i)$ is a function with 3 free parameters which parametrizes the dependence of the position of the centroid of each gaussian $x_i = f(A_i)$ on the isotope mass $A_i$,

  $$f(A_i) = a_0 + a_1 A_i + a_2 A_i^2$$

- $\mathcal{B}(x)$ is an *ad hoc* empirical background function used to account for experimental noise (continuous distribution of points in between the isotopes for different $Z$ in Fig. 6). In the present case, an exponential background was found to be suitable.

The results of the fitting procedure are superimposed on the data presented in Fig. 7 where the background contribution $\mathcal{B}(x)$ has been removed. An important advantage of this method is being able to identify isotopes with very low statistics, not immediately visible in the data. For example, the PID spectrum for carbon isotopes, $Z = 6$, displays 3 clear peaks and a shoulder for PID values around 5.8-5.9, corresponding to isotopes $A = 11 - 14$; the fit is however greatly improved by adding 2 further contributions at lower ($A = 10$) and higher ($A = 15$) PID values. The $A = 10$ isotope contribution is so small that it is only really visible using a logarithmic scale (inset in the figure). Similar results are observed for the oxygen isotopes, where in addition to the 3 main peaks ($A = 16 - 18$) the fit permits the additional assignment of isotopes $A = 15$ and $A = 19$, and for neon isotopes, for which a slight shoulder and long tail at the largest PID values can be assigned to the most neutron rich isotopes, $A = 23$ and $A = 24$.

In the offline analysis [36] the PID of each reconstructed particle is used to assign its mass number following a statistical prescription which respects the raw yields found from the fit and includes rejection of spurious background noise. The probability that a particle with given PID has mass $A_i$ is given by

$$P(A_i|x = \mathrm{PID}) = \frac{N_i}{y(x)} \mathcal{G}(x, f(A_i), \sigma) \tag{2}$$

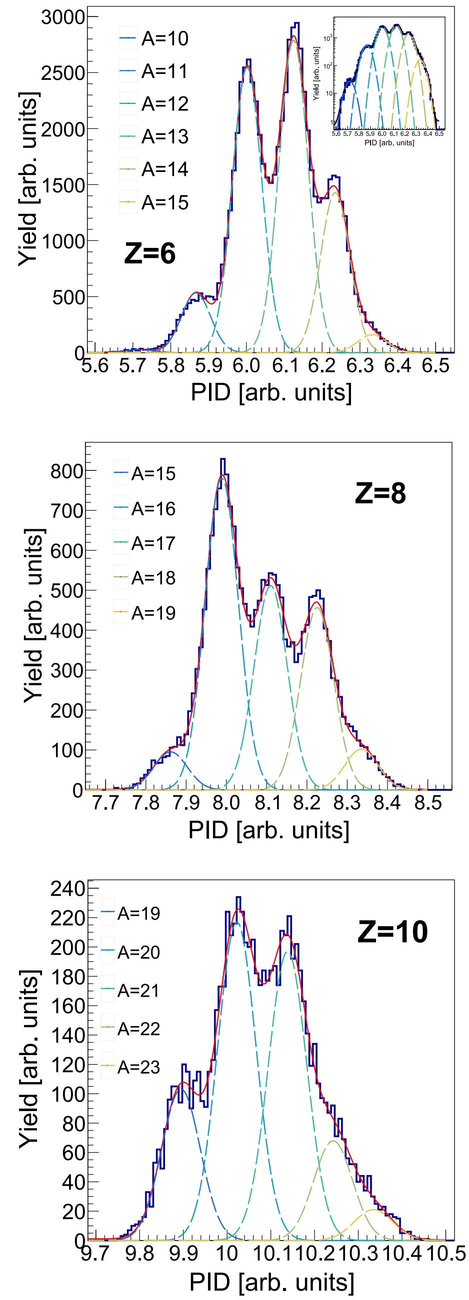


**Fig. 7.** Linearized PID spectra (see text) obtained for $Z = 6, 8, 10$ fragments stopping in telescope 3 of ring 6. Histograms represent the data, the red line is the fit using Eq. (1), the dashed curves represent the individual gaussians used for each isotope. For carbon isotopes, the inset presents the data with a logarithmic yield axis, in order to see the very low statistics $A = 10$ isotopes.

whereas the probability that the 'particle' is in fact just noise is given by

$$P(\mathrm{noise}|x = \mathrm{PID}) = \frac{\mathcal{B}(x)}{y(x)} \tag{3}$$

Each particle is therefore either assigned an isotopic mass number $A_i$ with probability Eq (2) or rejected as unidentifiable noise with probability Eq (3). The PID spectra in Fig. 7 were built using identified reconstructed particles, hence the background contribution has already been subtracted.

Fig. 8(a) shows the proportion of telescopes on each of rings 6 to 9 for which isotopic identification was achieved, as a function of the fragment charge, $Z$. It can be seen that isotopic identification up to oxygen ($Z = 8$) was achieved for the majority of telescopes on all rings, whereas at the most forward angles (rings 6,7), where the yield of heavier fragments is more important, identification up to neon ($Z = 10$) is common, while for ring 6 even magnesium isotopes ($Z = 12$) were identified in 50% of cases. It should be noted that although the detectors of rings 6 & 7 were brand new, those of rings 8 & 9 were mounted since at least 2007, if not before, and yet in both cases isotopic identification up to $Z = 8$ was achieved for the first time in these telescopes.

In order to quantify the quality of isotopic identification for all telescopes, we introduce a figure of merit (FoM) [37] based on the ratio between the separation of two adjacent centroids (isotopes) $x_i, x_j$ compared to the full-width half maximum of the peaks,

$$\mathcal{M}_{i,j} = \frac{x_j - x_i}{2\sqrt{2\ln 2}(\sigma_i + \sigma_j)} = \frac{x_j - x_i}{4\sqrt{2\ln 2}\sigma} \quad (4)$$

where $\sigma_i = \sigma_j = \sigma$ is the common gaussian width used to fit the isotopes of each element for each telescope, Eq. (1). This ratio has values $\mathcal{M}_{ij} > 0.5$ for peaks in PID spectra separated by more than the full width of the peaks at half-maximum.

As each element is associated with several isotopes/peaks, in order to calculate a representative FoM for each $Z$, we have calculated a mean value of $\mathcal{M}_{ij}$ using 3 isotopes, with indices $i = i_{\max} - 1$, $i_{\max}$ and $i_{\max} + 1$, where $i_{\max}$ is the index of the isotope with the largest yield in the fit of Eq. (1). Then we calculate for the figure of merit

$$\mathrm{FoM} = \frac{1}{2} \sum_{i=i_{\max}-1}^{i_{\max}} \frac{\mathcal{M}_{i,i+1}}{A_{i+1} - A_i} \quad (5)$$

where the denominator handles the case of adjacent isotopes with non-consecutive mass numbers (e.g. $^{7}$Be and $^{9}$Be).

Figs. 8(b)–(e) then show the FoM value achieved for fragments by $Z$ for the four rings equipped with Si-CsI telescopes. In each case the mean value for all 24 telescopes of the ring is given by the solid line, while the coloured area represents the range of FoM from the worst (smallest) to the best (largest) value for the ring. The results show a quite homogeneous mean identification quality for all $Z$ and (at least) rings 6 and 7. A more important variation of identification quality is observed for the older silicon detectors of rings 8 and 9. However it is important to underline that previously, only $Z$ identification was achieved with these telescopes; during E818 we obtained isotopic identification up to oxygen using the same old silicon wafers. Since these tests were performed, the silicon wafers of these rings have also been replaced with new detectors, therefore in future we expect a similar uniformity of isotopic identification for all rings.

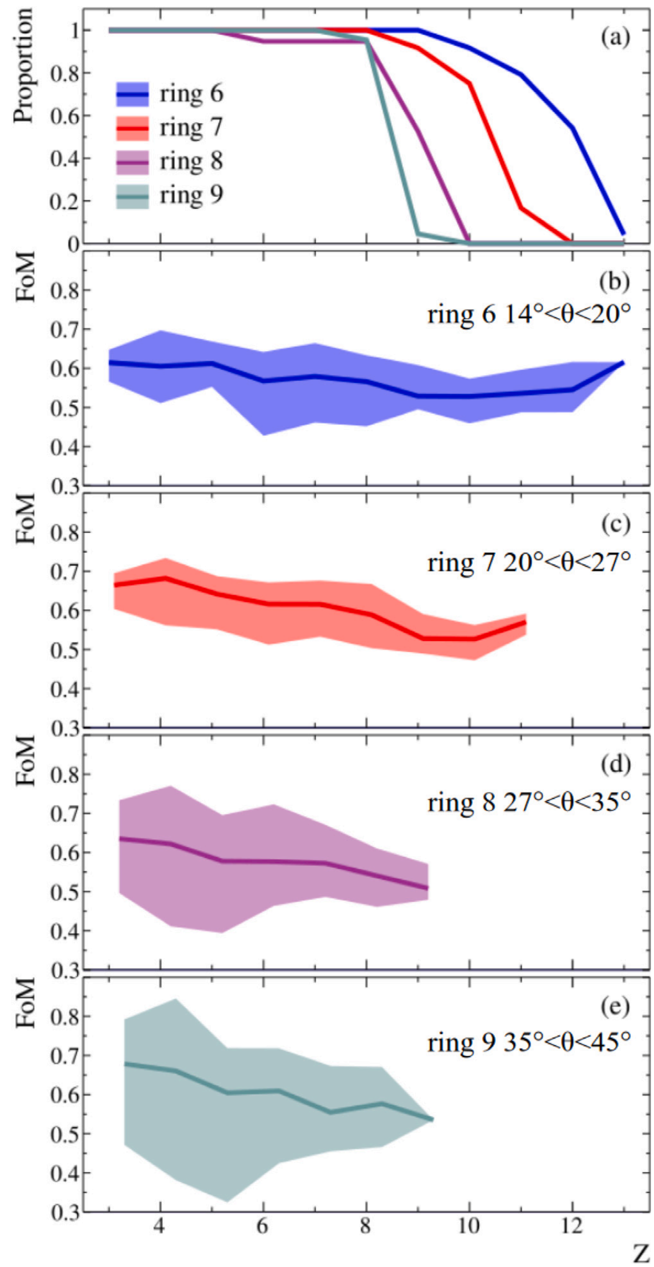


**Fig. 8.** Isotopic identification performances: (a) proportion of modules per ring with isotopic discrimination as a function of the fragment charge, $Z$; (b-e) $Z$ dependence of the quality of identification (FoM, see text) for INDRA rings 6 to 9, the polar angle coverage of each ring is given in the legends. The solid lines display the average FoM while the filled area limits shows the best and worst modules.

## 4. Summary and outlook

After 25 years of operation with dedicated, custom DAQ electronics based on the VXI standard developed at the beginning of the 1990s, INDRA now has new digital electronics using off-the-shelf modules provided by mesytec GmbH & Co. KG. At the same time, all low- and high-voltage supplies, in-air cabling and signal routings have also been replaced. The implementation of the new system is far more compact than before, occupying a single VME crate, and has resulted in an order of magnitude improvement of the DAQ dead time, facilitating the coupling of INDRA with other arrays, especially FAZIA. For E789 INDRA was basically a slave to FAZIA, with the result that the effective global trigger was a multiplicity of 2 fired telescopes in FAZIA, i.e. at very forward angles, below 14$^{o}$. As detailed in [38], such trigger conditions exert a large bias on the impact parameter distribution of the acquired reactions, making a model-independent reconstruction of the experimental centrality using the method of [39] almost impossible. For the E789 data it was only possible because a subset of the same reactions ($^{58}$Ni+$^{58}$Ni collisions at 32 and 52 MeV/u) had already been measured in 1994 using INDRA with a minimum bias trigger (multiplicity over the full angular range). From E818 onwards, operating INDRA and FAZIA together in common dead time means that we recover a minimally biased impact parameter distribution for the measured events, and the method of [39] can be applied even for reactions not previously measured with INDRA alone.

The digital signal processing with its automatic baseline restoration has significantly increased the energy resolution, allowing isotopic ($Z$ and $A$) identification of nuclear fragments up to $Z = 10{\sim}12$ for the first time with INDRA. A first experiment using the new setup was successfully conducted in 2022, and further experimental campaigns coupling INDRA and FAZIA at GANIL are underway. The first of these took place in Spring 2025, including experiment E884 which aims to extend the study of [40] which was made using data from E789. In [40] a specific study was made of events in which excited nickel-like quasiprojectiles undergo binary break-up in the exit channel, producing two intermediate mass fragments with $Z \geq 5$. The study indicated a longer timescale for these reactions, changing the degree of isospin equilibration and providing new constraints for isospin-dependent transport models. However, during E789 INDRA provided no isotopic identification for $Z \geq 5$ fragments, therefore the study had to be limited to the 40∼50 % of break-up events where both fragments were detected in FAZIA [40]. The results of E884 will extend this study to a range of reactions using a beam of $^{70}$Zn projectiles at 35 MeV/u impinging on targets of $^{27}$Al, $^{70}$Zn and $^{209}$Bi, and including the full set of break-up events even when one of the two fragments is detected and isotopically identified in INDRA. Such studies are only now possible with INDRA-FAZIA.

## CRediT authorship contribution statement

**J.D. Frankland:** Writing – original draft, Software, Investigation, Conceptualization. **N. Le Neindre:** Writing – original draft, Supervision, Project administration. **M. Henri:** Writing – review & editing, Validation, Project administration, Methodology, Investigation, Conceptualization. **C. Gouyet:** Validation, Methodology, Investigation, Conceptualization. **R. Revenko:** Supervision, Methodology, Investigation, Conceptualization. **Q. Fable:** Writing – review & editing, Project administration, Investigation, Data curation. **D. Gruyer:** Writing – review & editing, Writing – original draft, Validation, Software, Investigation, Formal analysis.

## Declaration of competing interest

The authors declare the following financial interests/personal relationships which may be considered as potential competing interests: Maxime Henri reports financial support was provided by Normandy Region. If there are other authors, they declare that they have no known competing financial interests or personal relationships that could have appeared to influence the work reported in this paper.

## Acknowledgements

The INDRA collaboration warmly acknowledges the Région Normandie for the grants supplied under the Réseaux d'Intérêts Normands (RIN) GANIL Innovation Future (GIF) n$^o$ 20E02583 and FAZIA INDRA Data for Nuclear Equation Of State (FIDNEOS) n$^o$ 18E01722 [41–43]. We also thank Navin Alahari and Héloise Goutte, respectively director and deputy director of GANIL at the time, for securing the RIN-GIF funding, as well as Marek Lewitowicz of GANIL who piloted the project. We warmly acknowledge the indispensable support of Robert Schneider, Florian Lüke and Gregor Montermann of mesytec GmbH & Co. KG with the implementation of the new DAQ electronics and software, as well as Antoine Lemasson and Frédéric Saillant of GANIL. We thank Claude Garrel for his expertise and exemplary work on the preparation of the cables and connectors. We would like to thank collectively the mechanical workshops of both GANIL and LPC Caen.

## Data availability

Data will be made available on request.

## References

[1] J. Pouthas, B. Borderie, R. Dayras, E. Plagnol, M. Rivet, F. Saint-Laurent, J. Steckmeyer, G. Auger, C. Bacri, S. Barbey, A. Barbier, A. Benkirane, J. Benlliure, B. Berthier, E. Bougamont, P. Bourgault, P. Box, R. Bzyl, B. Cahan, Y. Cassagnou, D. Charlet, J. Charvet, A. Chbihi, T. Clerc, N. Copinet, D. Cussol, M. Engrand, J. Gautier, Y. Huguet, O. Jouniaux, J. Laville, P. Le Botlan, A. Leconte, R. Legrain, P. Lelong, M. Le Guay, L. Martina, C. Mazur, P. Mosrin, L. Olivier, J. Passerieux, S. Pierre, B. Piquet, E. Plaige, E. Pollacco, B. Raine, A. Richard, J. Ropert, C. Spitaels, L. Stab, D. Sznajderman, L. Tassan-got, J. Tillier, M. Tripon, P. Vallerand, C. Volant, P. Volkov, J. Wieleczko, G. Wittwer, Nucl. Instrum. Methods Phys. Res. Sect. A: Accel. Spectrometers Detect. Assoc. Equip. 357 (2–3) (1995) 418–442, http://dx.doi.org/10.1016/0168-9002(94)01543-0, URL http://linkinghub.elsevier.com/retrieve/pii/0168900294015430.

[2] A. Ono, Prog. Part. Nucl. Phys. 105 (2019) 139–179, http://dx.doi.org/10.1016/j.ppnp.2018.11.001, https://linkinghub.elsevier.com/retrieve/pii/S0146641018300863.

[3] P. Danielewicz, R. Lacey, W.G. Lynch, Science 298 (5598) (2002) 1592–1596, http://dx.doi.org/10.1126/science.1078070, https://www.sciencemag.org/lookup/doi/10.1126/science.1078070.

[4] B. Borderie, J.D. Frankland, Prog. Part. Nucl. Phys. 105 (2019) 82–138, http://dx.doi.org/10.1016/j.ppnp.2018.12.002, URL https://linkinghub.elsevier.com/retrieve/pii/S0146641018301030.

[5] J. Pouthas, A. Bertaut, B. Borderie, P. Bourgault, B. Cahan, G. Carles, D. Charlet, D. Cussol, R. Dayras, M. Engrand, O. Jouniaux, P. Le Botlan, A. Leconte, P. Lelong, L. Martina, P. Mosrin, L. Olivier, J. Passerieux, B. Piquet, E. Plagnol, E. Plaige, B. Raine, A. Richard, F. Saint-Laurent, C. Spitaels, J. Tillier, M. Tripon, P. Vallerand, P. Volkov, G. Wittwer, Nucl. Instrum. Methods Phys. Res. Sect. A: Accel. Spectrometers Detect. Assoc. Equip. 369 (1) (1996) 222–247, http://dx.doi.org/10.1016/0168-9002(95)00770-9, http://linkinghub.elsevier.com/retrieve/pii/0168900295007709.

[6] J. Steckmeyer, D. Cussol, J. Duchon, J. Gautier, J. Laville, P. Le Botlan, A. Leconte, J. Lelandais, V. Métivier, P. Mosrin, E. Rosato, J. Tillier, A. Wieloch, Nucl. Instrum. Methods Phys. Res. Sect. A: Accel. Spectrometers Detect. Assoc. Equip. 361 (3) (1995) 472–481, http://dx.doi.org/10.1016/0168-9002(95)00203-0, URL https://linkinghub.elsevier.com/retrieve/pii/0168900295002030.

[7] O. Lopez, S. Piantelli, E789_18 - Isospin transport and the density dependence of the symmetry energy, 2019, http://dx.doi.org/10.26143/ganil-2019-e789_18, URL https://u.ganil-spiral2.eu/10.26143/GANIL-2019-E789_18.html.

[8] J. Łukasik, W. Trautmann, G. Auger, M.L. Begemann-Blaich, N. Bellaize, R. Bittiger, F. Bocage, B. Borderie, R. Bougault, B. Bouriquet, J.L. Charvet, A. Chbihi, R. Dayras, D. Durand, J.D. Frankland, E. Galichet, D. Gourio, D. Guinet, S. Hudan, B. Hurst, P. Lautesse, F. Lavaud, A. Le Fèvre, R. Legrain, O. Lopez, U. Lynen, W.F. Müller, L. Nalpas, H. Orth, E. Plagnol, E. Rosato, A. Saija, C. Sfienti, C. Schwarz, J.C. Steckmeyer, B. Tamain, A. Trzciński, K. Turzó, E. Vient, M. Vigilante, C. Volant, B. Zwiegliński, Prog. Part. Nucl. Phys. 53 (1) (2004) 77–80, http://dx.doi.org/10.1016/j.ppnp.2004.02.013.

[9] Q. Fable, A. Chbihi, M. Boisjoli, J.D. Frankland, A. Le Fèvre, N. Le Neindre, P. Marini, G. Verde, G. Ademard, L. Bardelli, C. Bhattacharya, S. Bhattacharya, E. Bonnet, B. Borderie, R. Bougault, G. Casini, M. La Commara, R. Dayras, J.E. Ducret, F. Farget, E. Galichet, T. Génard, F. Gramegna, D. Gruyer, M. Henri, S. Kundu, J. Lemarié, O. Lopez, J. Łukasik, L. Manduci, J. Moisan, G. Mukherjee, P. Napolitani, A. Olmi, M. Pârlog, S. Piantelli, G. Poggi, A. Rebillard-Soulié, R. Roy, B. Sorgunlu, S. Velardita, E. Vient, M. Vigilante, J.P. Wieleczko, Phys. Rev. C 106 (2) (2022) 024605, http://dx.doi.org/10.1103/PhysRevC.106.024605, arXiv:2202.13850.

[10] Q. Fable, A. Chbihi, J.D. Frankland, P. Napolitani, G. Verde, E. Bonnet, B. Borderie, R. Bougault, E. Galichet, T. Génard, D. Gruyer, M. Henri, M. La Commara, A. Le Fèvre, J. Lemarié, N. Le Neindre, O. Lopez, P. Marini, M. Pârlog, A. Rebillard-Soulié, W. Trautmann, E. Vient, M. Vigilante, Phys. Rev. C 107 (1) (2023) 014604, http://dx.doi.org/10.1103/PhysRevC.107.014604, URL https://link.aps.org/doi/10.1103/PhysRevC.107.014604.

[11] M. Morjean, D. Jacquet, J.L. Charvet, A. L'Hoir, M. Laget, M. Parlog, A. Chbihi, M. Chevallier, C. Cohen, D. Dauvergne, R. Dayras, A. Drouart, C. Escano-Rodriguez, J.D. Frankland, R. Kirsch, P. Lautesse, L. Nalpas, C. Ray, C. Schmitt, C. Stodel, L. Tassan-Got, E. Testa, C. Volant, Phys. Rev. Lett. 101 (7) (2008) http://dx.doi.org/10.1103/PhysRevLett.101.072701.

[12] R. Bougault, G. Casini, E818_20 - Extending our knowledge of Warm Dense Nuclear Matter in the low density region, 2022, http://dx.doi.org/10.26143/GANIL-2022-E818_20, URL https://u.ganil-spiral2.eu/10.26143/GANIL-2022-E818_20.html.

[13] mesytec MDPP-32 module (mesytec GmbH & Co. KG), URL https://www.mesytec.com/products/nuclear-physics/MDPP-32.htm.

[14] R. Schneider, Mesytec GmbH & Co. KG private communication, 2025.

[15] mesytec MVLC module (mesytec GmbH & Co. KG)), URL https://www.mesytec.com/products/nuclear-physics/MVLC.html.

[16] mesytec VME data acquisition software (mesytec GmbH & Co. KG), URL https://www.mesytec.com/downloads/mvme.html.
[17] X. Grave, R. Canedo, J.-F. Clavelin, S. Du, E. Legay, 14th IEEE-NPSS Real Time Conference, 2005, 2005, p. 5, http://dx.doi.org/10.1109/RTC.2005.1547454.
[18] MFM: Multiframe Metaformat binary formats for data acquisition, URL https://informatique.in2p3.fr/?q=mfm.
[19] ZeroMQ: An open-source universal messaging library, URL https://zeromq.org/.
[20] mesytec data parsing library & GANIL acquisition interface, URL https://gitlab.in2p3.fr/mesytec-ganil/mesytec_data.
[21] NARVAL ZMQ receiver actor URL https://gitlab.in2p3.fr/ganil/zmq-receiver.
[22] S. Valdré, G. Casini, N. Le Neindre, M. Bini, A. Boiano, B. Borderie, P. Edelbruck, G. Poggi, F. Salomon, G. Tortone, R. Alba, S. Barlini, E. Bonnet, B. Bougard, R. Bougault, G. Brulin, M. Bruno, A. Buccola, A. Camaiani, A. Chbihi, C. Ciampi, M. Cicerchia, M. Cinausero, D. Dell'Aquila, P. Desrues, J. Dueñas, D. Fabris, M. Falorsi, J. Frankland, C. Frosin, E. Galichet, R. Giordano, F. Gramegna, L. Grassi, D. Gruyer, M. Guerzoni, M. Henri, M. Kajetanowicz, K. Korcyl, A. Kordyasz, T. Kozik, P. Lecomte, I. Lombardo, O. Lopez, C. Maiolino, G. Mantovani, T. Marchi, A. Margotti, Y. Merrer, L. Morelli, A. Olmi, A. Ordine, P. Ottanelli, C. Pain, M. Pałka, M. Pârlog, G. Pasquali, G. Pastore, S. Piantelli, H. de Préaumont, R. Revenko, A. Richard, M. Rivet, J. Ropert, E. Rosato, F. Saillant, D. Santonocito, E. Scarlini, S. Serra, C. Soulet, G. Spadaccini, A. Stefanini, G. Tobia, S. Upadhyaya, A. Vanzanella, G. Verde, E. Vient, M. Vigilante, E. Wanlin, G. Wittwer, A. Zucchini, Nucl. Instrum. Methods Phys. Res. Sect. A: Accel. Spectrometers Detect. Assoc. Equip. 930 (2019) 27–36, http://dx.doi.org/10.1016/j.nima.2019.03.082, URL https://linkinghub.elsevier.com/retrieve/pii/S0168900219304243.
[23] G. Wittwer, CENTRUM: Clock event number transmitter receiver universal module, 2004.
[24] MFM Merger for GANIL Data Flow, URL https://gitlab.in2p3.fr/ganil/mfm-merger.
[25] CAEN SY4527 Universal Multichannel Power Supply System Mainframe (CAEN S.p.A.), URL https://www.caen.it/products/SY4527.
[26] CAEN A7030N 48 channel 3 kV negative power supply (CAEN S.p.A.), URL https://www.caen.it/products/a7030.
[27] CAEN A7040N 48 channel 100 V negative power supply (CAEN S.p.A.), URL https://www.caen.it/products/a7040.
[28] CAEN A1542DN 12 channel -500 V negative power supply (CAEN S.p.A.), URL https://www.caen.it/products/a1542.
[29] CAEN A2519A 8 channel 15 V low voltage supply (CAEN S.p.A.), URL https://www.caen.it/products/a2519.
[30] ATOS Racks: an expert in packaging products for the electronics industry (ATOS company), URL https://atos-racks.com/.
[31] Agilink Group: your smart connection (Ivry Interconnect Services), URL https://www.agilink-group.fr.
[32] Socapex connectors 29 pins 12729XLM1U & 12729XLF1U and 53 pins 12753XLF1U & 12753XLM1U (Amphenol Corporation), URL https://amphenol-socapex.com.
[33] C. Ciampi, S. Piantelli, G. Casini, G. Pasquali, J. Quicray, L. Baldesi, S. Barlini, B. Borderie, R. Bougault, A. Camaiani, A. Chbihi, D. Dell'Aquila, M. Cicerchia, J.A. Dueñas, Q. Fable, D. Fabris, J.D. Frankland, C. Frosin, T. Génard, F. Gramegna, D. Gruyer, M. Henri, B. Hong, S. Kim, A. Kordyasz, T. Kozik, M.J. Kweon, J. Lemarié, N. Le Neindre, I. Lombardo, O. Lopez, T. Marchi, S.H. Nam, A. Ordine, P. Ottanelli, J. Park, J.H. Park, M. Pârlog, G. Poggi, A. Rebillard-Soulié, A.A. Stefanini, S. Upadhyaya, S. Valdré, G. Verde, E. Vient, M. Vigilante, Phys. Rev. C 106 (2) (2022) 024603, http://dx.doi.org/10.1103/PhysRevC.106.024603.
[34] M. Pârlog, B. Borderie, M. Rivet, G. Tabacaru, A. Chbihi, M. Elouardi, N. Le Neindre, O. Lopez, E. Plagnol, L. Tassan-Got, G. Auger, C. Bacri, N. Bellaize, F. Bocage, R. Bougault, B. Bouriquet, R. Brou, P. Buchet, J. Charvet, J. Colin, D. Cussol, R. Dayras, A. Demeyer, D. Doré, D. Durand, J. Frankland, E. Galichet, E. Genouin-Duhamel, E. Gerlic, S. Hudan, D. Guinet, P. Lautesse, F. Lavaud, J. Laville, J. Lecolley, C. Leduc, R. Legrain, M. Louvel, A. Maskay, L. Nalpas, J. Normand, J. Péter, E. Rosato, F. Saint-Laurent, J. Steckmeyer, B. Tamain, O. Tirel, E. Vient, C. Volant, J. Wieleczko, Nucl. Instrum. Methods Phys. Res. Sect. A: Accel. Spectrometers Detect. Assoc. Equip. 482 (3) (2002) 693–706, http://dx.doi.org/10.1016/S0168-9002(01)01712-0, URL http://linkinghub.elsevier.com/retrieve/pii/S0168900201017120.
[35] D. Gruyer, E. Bonnet, A. Chbihi, J. Frankland, S. Barlini, B. Borderie, R. Bougault, J. Dueñas, E. Galichet, A. Kordyasz, T. Kozik, N. Le Neindre, O. Lopez, M. Pârlog, G. Pastore, S. Piantelli, S. Valdré, G. Verde, E. Vient, Nucl. Instrum. Methods Phys. Res. Sect. A: Accel. Spectrometers Detect. Assoc. Equip. 847 (2017) 142–147, http://dx.doi.org/10.1016/j.nima.2016.11.062, URL https://linkinghub.elsevier.com/retrieve/pii/S016890021631230X.
[36] J.D. Frankland, D. Gruyer, E. Bonnet, KaliVeda heavy-ion analysis toolkit, Toolkit for analysis & simulation of Fermi energy heavy-ion collisions, URL https://kaliveda.in2p3.fr, http://dx.doi.org/10.5281/zenodo.7664900.
[37] G. Pastore, D. Gruyer, P. Ottanelli, N. Le Neindre, G. Pasquali, R. Alba, S. Barlini, M. Bini, E. Bonnet, B. Borderie, R. Bougault, M. Bruno, G. Casini, A. Chbihi, D. Dell'Aquila, J. Dueñas, D. Fabris, L. Francalanza, J. Frankland, F. Gramegna, M. Henri, A. Kordyasz, T. Kozik, I. Lombardo, O. Lopez, L. Morelli, A. Olmi, M. Pârlog, S. Piantelli, G. Poggi, D. Santonocito, A. Stefanini, S. Valdré, G. Verde, E. Vient, M. Vigilante, Nucl. Instrum. Methods Phys. Res. Sect. A: Accel. Spectrometers Detect. Assoc. Equip. 860 (2017) 42–50, http://dx.doi.org/10.1016/j.nima.2017.01.048, URL https://linkinghub.elsevier.com/retrieve/pii/S0168900217301092.
[38] C. Ciampi, J.D. Frankland, D. Gruyer, N. Le Neindre, S. Mallik, R. Bougault, A. Chbihi, L. Baldesi, S. Barlini, E. Bonnet, B. Borderie, A. Camaiani, G. Casini, I. Dekhissi, D. Dell'Aquila, J.A. Dueñas, Q. Fable, F. Gramegna, C. Gouyet, M. Henri, B. Hong, S. Kim, A. Kordyasz, T. Kozik, M.J. Kweon, I. Lombardo, O. Lopez, L. Manduci, T. Marchi, K. Mazurek, S.H. Nam, J. Park, M. Pârlog, G. Pasquali, S. Piantelli, G. Poggi, A. Rebillard-Soulié, R. Revenko, S. Valdré, G. Verde, E. Vient, INDRA-FAZIA Collaboration Collaboration, Phys. Rev. C 111 (2025) 044601, http://dx.doi.org/10.1103/PhysRevC.111.044601.
[39] J.D. Frankland, D. Gruyer, E. Bonnet, B. Borderie, R. Bougault, A. Chbihi, J.E. Ducret, D. Durand, Q. Fable, M. Henri, J. Lemarié, N. Le Neindre, I. Lombardo, O. Lopez, L. Manduci, M. Pârlog, J. Quicray, G. Verde, E. Vient, M. Vigilante, Phys. Rev. C 104 (3) (2021) 034609, http://dx.doi.org/10.1103/PhysRevC.104.034609.
[40] C. Ciampi, S. Piantelli, G. Casini, A. Ono, J.D. Frankland, L. Baldesi, S. Barlini, B. Borderie, R. Bougault, A. Camaiani, A. Chbihi, J.A. Dueñas, Q. Fable, D. Fabris, C. Frosin, T. Génard, F. Gramegna, D. Gruyer, M. Henri, B. Hong, S. Kim, A. Kordyasz, T. Kozik, M.J. Kweon, N. Le Neindre, I. Lombardo, O. Lopez, T. Marchi, K. Mazurek, S.H. Nam, J. Park, M. Pârlog, G. Pasquali, G. Poggi, A. Rebillard-Soulié, A.A. Stefanini, S. Upadhyaya, S. Valdré, G. Verde, E. Vient, M. Vigilante, Phys. Rev. C 108 (5) (2023) 054611, http://dx.doi.org/10.1103/PhysRevC.108.054611.
[41] Réseaux d'intérêts Normands (Région Normandie), URL https://www.normandie.fr/aides-regionales.
[42] Normandie Université, Université de Caen, appels à projets régionaux (Normandie Université), URL https://www.normandie-univ.fr/recherche/appels-a-projets/appels-regionaux.
[43] FIDNEOS: FAZIA INDRA Data for Nuclear Equation Of State (Région Normandie, Normandie Université, LPC Caen), URL https://www.lpc-caen.in2p3.fr/recherche/physique-nucleaire/dynamique-thermodynamique-nucleaire/projet-fidneos/.